

A Comparative Study on the Radiation Attenuation Properties of Iron and Stony Meteorites: A Case of Mundrabilla and NWA 7629 Meteorites

Canel Eke*

Department of Mathematics and Science Education, Faculty of Education,
Akdeniz University, 07058 Antalya, Turkey

*Corresponding author: ceke@akdeniz.edu.tr, caneleke@hotmail.com

Published online: 25 August 2022

To cite this article: Eke, C. (2022). A comparative study on the radiation attenuation properties of iron and stony meteorites: A case of Mundrabilla and NWA 7629 meteorites. *J. Phys. Sci.*, 33(2), 77–93. <https://doi.org/10.21315/jps2022.33.2.5>

To link to this article: <https://doi.org/10.21315/jps2022.33.2.5>

ABSTRACT: *The goal of this paper is to compare and investigate the radiation attenuation properties of Mundrabilla and NWA 7629 meteorites in terms of the photon, fast neutron and charged particles. The linear attenuation coefficients of Mundrabilla are higher than those of NWA 7629. The half value layers, tenth value layers and mean free paths of NWA 7629 are greater than those of Mundrabilla. The effective atomic number, effective electron density, equivalent atomic number and effective conductivity of the Mundrabilla are nearly constant between 0.015 MeV–15 MeV. Both the exposure build-up factors and energy absorption build-up factors are maximum at 0.8 MeV for Mundrabilla and NWA 7629. The projected/ continuous-slowing-down approximation (CSDA) ranges for charged particles for NWA 7629 are higher than those of Mundrabilla. The fast neutron attenuation of Mundrabilla is better than those of NWA 7629. Consequently, it can be concluded that photon, fast neutron and charged particles attenuation capability of Mundrabilla are better than NWA 7629 due to the nickel content, higher density and higher content of iron.*

Keywords: Mundrabilla meteorite, NWA 7629 meteorite, photon attenuation, fast neutron attenuation, charged particles attenuation

1. INTRODUCTION

Meteorites contain little components that are residuals from asteroids and rocks following several operations such as frictional warming, superficies fusing and volatilisation in the atmosphere. Meteorites arrive from outer space to the

atmosphere of the earth and these pieces ensure knowledge about the solar system.^{1,2} Since they are fragments of rock and metal that reach the surface of the Earth from outer space, they carry a record of the bombardment by cosmic rays which they have undergone.³ This information about conditions, in the form of radioactive and stable nuclei generated by transformation, is greatly protected by meteorites due to their chemical and physical constancy. Furthermore, the effects of cosmic rays on meteorites are similar to the produced effects of cosmic rays on Earth's atmosphere.³

Meteorites are different in physical and chemical characteristics such as mineralogy, petrology, whole-rock chemistry and oxygen isotopes. Meteorites are classified as iron meteorites, stony meteorites and stony-iron meteorites based on their components of metals, iron-nickel and silicates.^{1,4-6} Iron meteorites such as hexahedrites, octahedrites and ataxites are essentially iron-nickel alloys and they have no silicate. Stony meteorites such as chondrites, carbonaceous chondrites and achondrites make up most of the meteorites which come down to earth. Chondrites are similar in terms of contents to the earth's crust and mantle, while iron-stony meteorites such as pallasites and mesosiderites are mixtures of iron and stony type and are composed of silicate and metal phases.^{5,6}

Determination of various properties like contents of the components, mineralogy, petrology and oxygen isotopes are considerable for the classification of meteorites.⁷ For example, Kosice meteorite was studied in terms of mineralogy, petrography, geochemistry and categorising by Ozdin et al.⁸ Various meteorites with different elemental contents were surveyed by laser-induced breakdown spectroscopy method by Dell'Aglia et al. and Clayton et al. categorised the meteorites in terms of oxygen isotope abundance.^{9,10} Kamargaon (L6) meteorite properties such as petrography, categorisation, oxygen isotopes, noble gases and cosmogenic enrolments were investigated by Ray et al. and Gemelli et al. researched iron meteorites using a hand-held x-ray fluorescence spectrometer.^{11,12} X-ray computed tomography imaging was employed for meteorite research as a nondestructive method as pointed out by Sears et al.¹³ Furthermore, cosmogenic radionuclides in meteorites were examined by Alexeev et al. and Komura et al.^{14,15}

Gamma-ray interaction with materials to assess the physical and chemical features of surfaces and objects of space such as soils and rocks has long been used as an influential instrument in various space duties for in situ measurements. The transmission method of photon is employed as a non-destructive method in calculations of soil and rock properties like water content, porosity and bulk density in geoscience.¹⁶⁻²⁴ Besides, gamma-ray spectrometry is utilised in space

studies to determine various properties of objects. For example, Peplowski et al. studied close to superficial elemental sheeting on Mars using gamma-ray spectrometry.²⁵ Addition to specifying burial depth and notional content of the sheets, they also need information about vertical and horizontal mobility in the water component of the near superficial materials, the regional galactic cosmic ray medium such as magnitude and energy dispersion, the depending on the flux of deep neutron, the cross section of gamma-ray production, content and column density of the atmosphere.²⁵ Consequently, experimental and modelling results of Peplowski et al. ensured a base for investigating the benefit of utilising orbiter and lander-based gamma-ray calculations to define sub-superficial deposits on Mars.²⁵ Evans et al. determined chlorine on the Mercury surface to investigate its impact on the planet's genesis and evolution using Mercury Surface, Space Environment, Geochemistry and Ranging (Messenger) spacecraft that owned gamma-ray neutron spectrometer and they declared that the prosperity of chlorine on the Mercury superficial has been specified for the initial time using Messenger spacecraft gamma-ray spectrometer and thermal neutron absorption displays increment in north polar area of Mercury, an outcome in agreement with the boosted chlorine prosperities.²⁶ Peplowski et al. studied geochemical regions of the northern hemisphere of Mercury using Messenger neutron evaluations, so they firstly mapped alterations in several thermal-neutron absorption elements using anti-coincidence shelter on the gamma-ray spectrometer of Messenger.²⁷ Lawrence et al. investigated the elemental composition of terranes of Mercury using Messenger spacecraft neutron spectrometer basis on the neutron transport simulation and fast neutrons flux of Mercury from 20°S to the north pole distance.²⁸ They noticed that cosmic ray-induced fast neutrons ensure a calculation of mean atomic mass and their results were convenient with previous works of Moon and Vesta.²⁸ Beck et al. tried to construct a comprehensive bulk chemistry data set of howardite, eucrite and diogenite to determine gamma-ray/neutron parameters, fast neutron counts, the cross-section of macroscopic thermal neutron attenuation, high energy gamma-ray composition parameters and iron abundance to compare with Dawn data.²⁹ They reported that these data can be used to differentiate howardite, eucrite and diogenite mobility on the asteroid 4 vesta surface.²⁹

In the scientific literature, photon attenuation characteristic of assorted matters such as elements, mixtures, compounds, soil samples, sand samples, medicinal and aromatic plants, granites and marbles, rocks, clay samples, concretes, polymers, various glass systems, etc., are investigated using theoretical simulation and experimental methods.^{30–53}

In addition to these studies, Komura et al. examined gamma-ray energy absorption build-up factors (EABF) of samples from the Earth, Moon and Mars related to penetration depth theoretically, by weighing the fraction of the component elements.¹⁵ The results of this study demonstrated that the samples from Earth have the biggest EABF while samples from Mars have the smallest EABF.¹⁵ Apart from that, there is no considerable difference in EABF of the materials from Earth, Moon and Mars.¹⁶ Kim et al. investigated theoretically radiation attenuation characteristics of Martian meteorites and Martian regolith to crosscheck their application as shields for improved manned assignments to Mars.⁵⁴ Consequently they pointed out that there is no significant effect in varying the contents of subgroups of Martian rocks on the shielding characteristics due to the identities of their contents but the addition of hydrogenous contents to Martian regolith increases shielding characteristics.⁵⁴ Moreira and Appoloni calculated theoretically mass attenuation coefficient (μ/ρ) of Earth, Moon and Mars materials between 1 keV to 100 GeV and they obtained that μ/ρ values were almost similar for higher energies than 100 keV though there are prominent distinctions among the studied samples at lower than 25 keV.⁵⁵

Radiation interacts with meteorites when the high energy proton and nuclides consist of the other charged nuclei move into its surface from every direction and cross through the material. As a result, new particles occur in different energies and types.⁵⁶ Occurred secondary particles pass many interactions and this gradual process proceeds until the energy is radiated. High energy protons of primary and secondary declining, neutrons for all energies are significant for condensed material as meteorites. Many data set about cosmic radiation occur primarily of high energy protons, with a significant ingredient of alpha particles and a little part of heavier nuclei in the area of space near the Earth.⁵⁶

Both humans and spacecraft equipment are below danger substantial detrimental effect due to the natural ionising radiation environment. Ionising radiation environments are occurred solar energetic particles up to a few 100 MeV and galactic cosmic rays with billion electron volt energies.⁵⁷ Therefore, radiation shielding materials are required for thermal shielding, biological shielding and instrument shielding.⁵⁸⁻⁶²

For that reason, the goal of this paper is to compare and research photon, fast neutron and charged particle attenuation characteristics of some Mundrabilla and NWA 7629 meteorites to evaluate the radiation shielding effect and evaluate whether there is a variation in attenuation properties of the classification of meteorites as well as contribute the scientific literature.

2. MATERIALS AND METHOD

In this study, radiation attenuation characteristics of Mundrabilla and NWA 7629 meteorites were investigated. These meteorites were selected from Nabawy and Rochette's work and they determined the content of the components of Mundrabilla and NWA 7629 meteorites using EDX method.² The reason for selecting these two meteorites is that Mundrabilla is a type of iron meteorite and NWA 7629 is a stony meteorite. The elemental contents and bulk density of the Mundrabilla and NWA 7629 meteorites are given in Table 1. Details of Mundrabilla and NWA 7629 meteorites can be found in Nabawy and Rochette.²

Table 1. Meteorite name, elements contents and densities of the Mundrabilla and NWA 7629 meteorites. (Data are taken from Nabawy and Rochette²)

Meteorite name	Elements contents (wt%)							Bulk density (g/cm ³)
	Fe	Ni	O	Mg	Si	Cl	Cr	
Mundrabilla	68.95	31.05	–	–	–	–	–	7.5608
NWA 7629	10.55	–	17.08	9.14	45.49	7.65	10.09	3.3830

To determine photon attenuation properties of Mundrabilla and NWA 7629 meteorites, linear attenuation coefficient (μ), μ/ρ , half value layer (HVL), tenth value layer (TVL), mean free path (MFP), radiation protection efficiency (RPE), effective atomic number (Z_{eff}), effective electron density (N_{eff}), equivalent atomic number (Z_{eq}), effective conductivity (C_{eff}), exposure build-up factor (EBF) and EABF as well as fast neutron removal cross-section (FNRC) were calculated theoretically using Phy-X/PSD software developed by Sakar et al. and theoretical equations for the calculations can be found in Sakar et al.⁶³ To calculate RPE values of Mundrabilla and NWA 7629, the thickness of the sample was assumed 1 cm. Furthermore, mass stopping power (MSP) and projected/CSDA range of Mundrabilla and NWA 7629 meteorites for charged particles (electron, proton, alpha and carbon) were obtained using ESTAR and SRIM software. Continuous slowing down approximation (CSDA) range is defined as the mean length displacement by a charged particle and the projected range (PR) is described as the mean displacement along the initial particle direction.^{64–68}

3. RESULTS AND DISCUSSION

The μ and μ/ρ of Mundrabilla and NWA 7629 meteorites descend with enhancing gamma-ray energy due to photoelectric influence, Compton scattering and pair production as seen in Figure 1. The photoelectric effect is the primary treatment at smaller gamma-ray energies, Compton scattering is effective at the medium

energies and at greater gamma-ray energies, pair production is dominant.⁶⁹ The μ and μ/ρ of Mundrabilla and NWA 7629 meteorites are the lowest at 15 MeV and they are the highest at 0.01 MeV. The μ values of Mundrabilla are higher than the μ values of NWA 7629 (as shown in Figure 1[a]). The μ/ρ values of Mundrabilla are greater than the μ/ρ values of NWA 7629 between 0.015 MeV and 0.3 MeV, there are no prominent variations between μ/ρ values of Mundrabilla and NWA 7629 between 0.4 MeV and 3 MeV, then again, the μ/ρ values of Mundrabilla are greater than the μ/ρ values of NWA 7629 up to 15 MeV (as shown in Figure 1[b]).

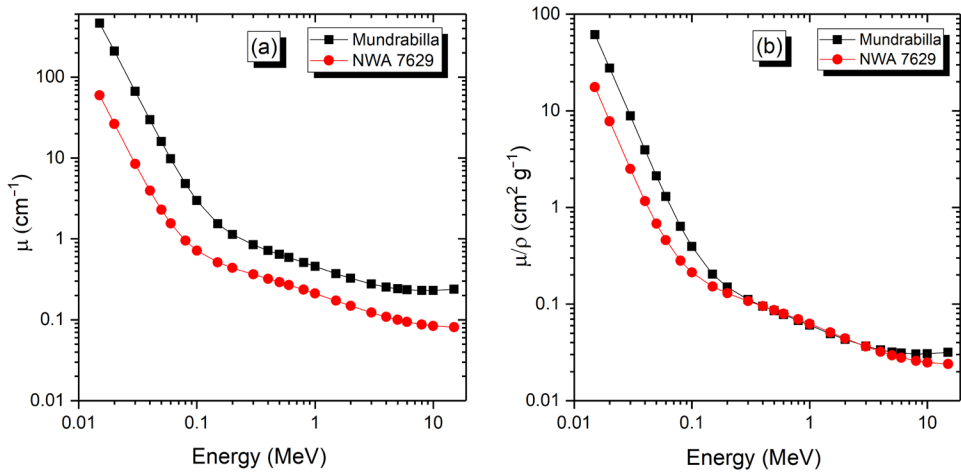


Figure 1: (a) μ and (b) μ/ρ as a function of photon energy for the Mundrabilla and NWA 7629 meteorites.

The HVLs, TVLs and MFPs of NWA 7629 are greater than those of Mundrabilla as presented Figures 2(a), 2(b) and 2(c), respectively. The RPEs of the Mundrabilla are higher than the RPEs of the NWA 7629 as shown in Figure 2(d). The HVLs, TVLs and MFPs of Mundrabilla and NWA 7629 enhance as photon energy increases whereas the RPEs of Mundrabilla and NWA 7629 decline as photon energy enhances. Consequently, it can be concluded that photon attenuation capability of Mundrabilla is greater than NWA 7629 due to the nickel content, higher content of iron and higher density.

The Z_{eff} and N_{eff} of the Mundrabilla are nearly constant among 0.015 MeV–15 MeV. Those of the NWA 7629 decline gradually between 0.015 MeV and 1 MeV afterwards they increase gradually up to 15 MeV (as shown in Figure 3). The Z_{eff} values vary similar to N_{eff} values for Mundrabilla and NWA 7629 in the examined energies.

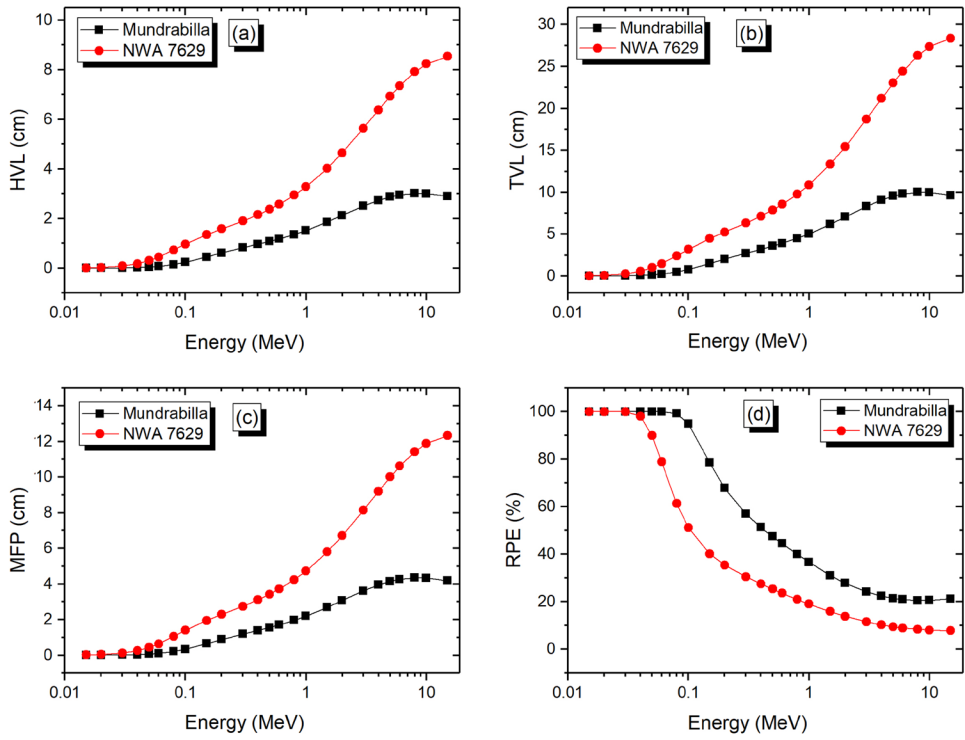


Figure 2: (a) HVL, (b) TVL, (c) MFP and (d) RPE as a function of photon energy for the Mundrabilla and NWA 7629 meteorites.

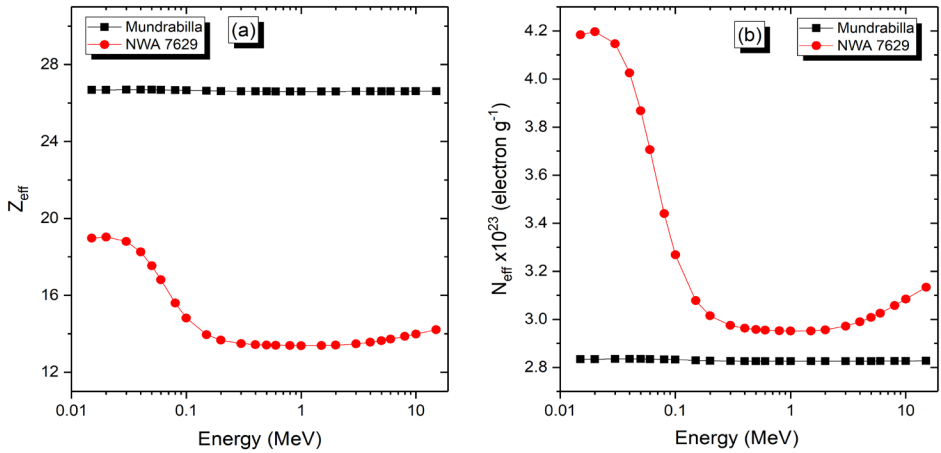


Figure 3: (a) Z_{eff} and (b) N_{eff} as a function of photon energy for the Mundrabilla and NWA 7629 meteorites.

Besides, the Z_{eq} and C_{eff} values are almost constant for Mundrabilla among 0.015 MeV–15 MeV as displayed in Figures 4(a) and 4(b), respectively. The Z_{eq} values of NWA 7629 rise progressively between 0.015 MeV and 1 MeV, subsequently, they decrease sharply at 1.5 MeV then they continue to decline slightly up to 15 MeV. The C_{eff} values of NWA 7629 tend to descend by stages between 0.015 MeV and 2 MeV, later they tend to ascend by stages up to 15 MeV.

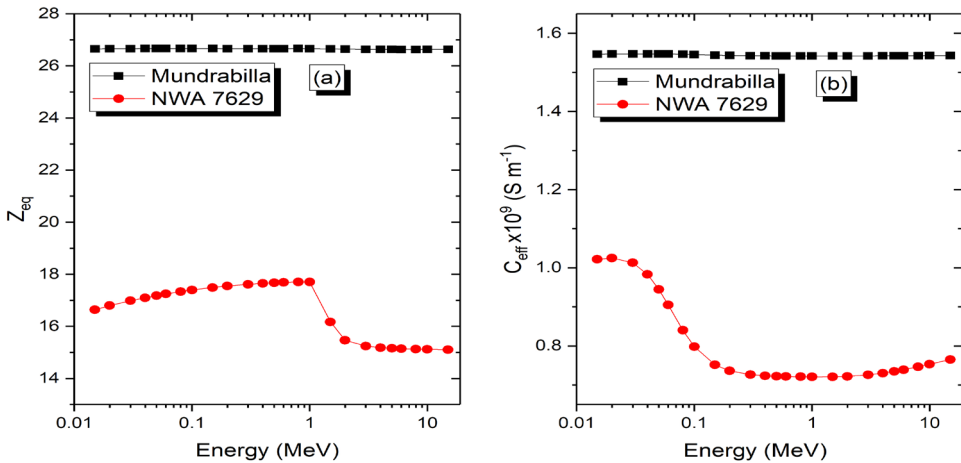


Figure 4: (a) Z_{eq} and (b) C_{eff} as a function of photon energy for the Mundrabilla and NWA 7629 meteorites.

Both the EBFs and EABFs are maximum at 0.8 MeV for Mundrabilla and NWA 7629 are illustrated in Figures 5 and 6, respectively. The EBFs and EABFs enhance between 0.015 MeV and 0.8 MeV, and then they decline up to 15 MeV. The EBFs and EABFs decrease from 20 mfp to 1 mfp for both Mundrabilla and NWA 7629.

The MSPs for electron decline as energy enhances for Mundrabilla and NWA 7629 (as shown in Figure 7). The MSPs of NWA 7629 for electrons are higher than the MSPs of Mundrabilla for electrons up to 8 MeV however, at 9 MeV and 10 MeV energies, the MSPs of Mundrabilla for electrons are higher than the MSPs of NWA 7629. The MSPs for the proton of Mundrabilla and NWA 7629 enhance up to 0.11 MeV and 0.12 MeV, then they decline up to 10 MeV (as shown in Figure 7). The MSPs for the alpha of Mundrabilla and NWA 7629 ascend up to 0.7 MeV and 0.8 MeV, afterwards they decline up to 10 MeV. The MSPs for the carbon of Mundrabilla and NWA 7629 rise up to 6 MeV and 6.5 MeV, subsequently they decline up to 10 MeV. The MSPs for proton, alpha and carbon of NWA 7629 are higher than that of Mundrabilla.

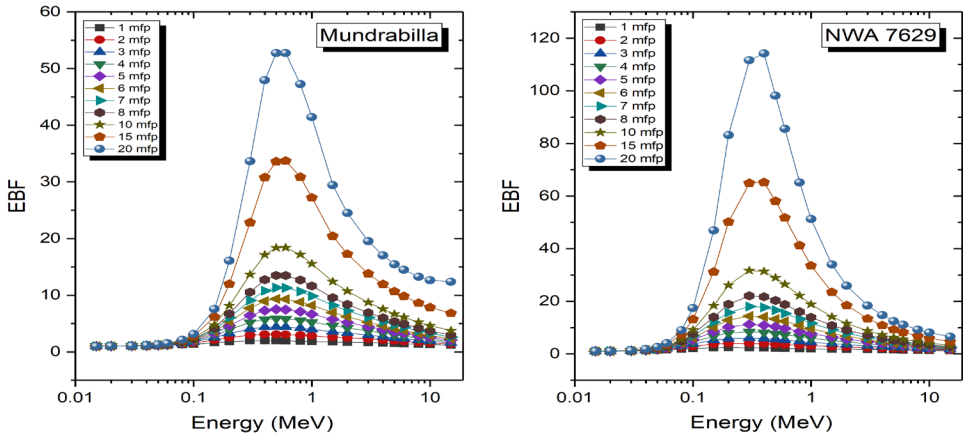


Figure 5: The EBF as a function of photon energy for the Mundrabilla and NWA 7629 meteorites.

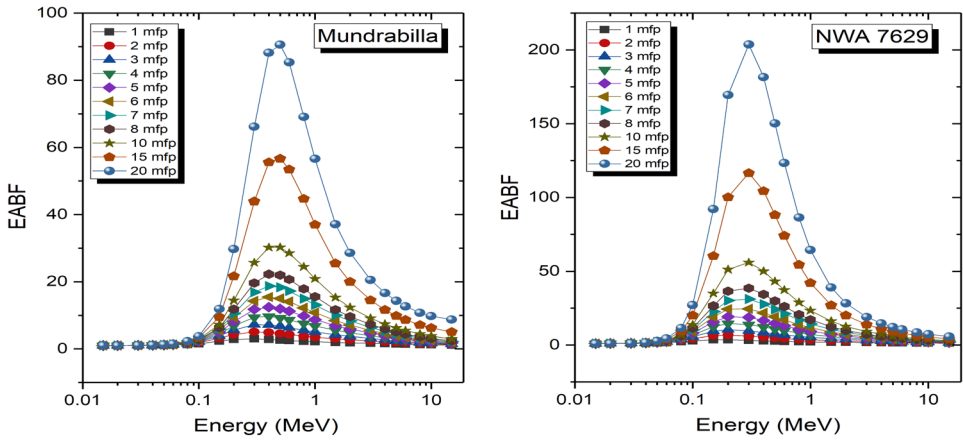


Figure 6: The EABF as a function of photon energy for the Mundrabilla and NWA 7629 meteorites.

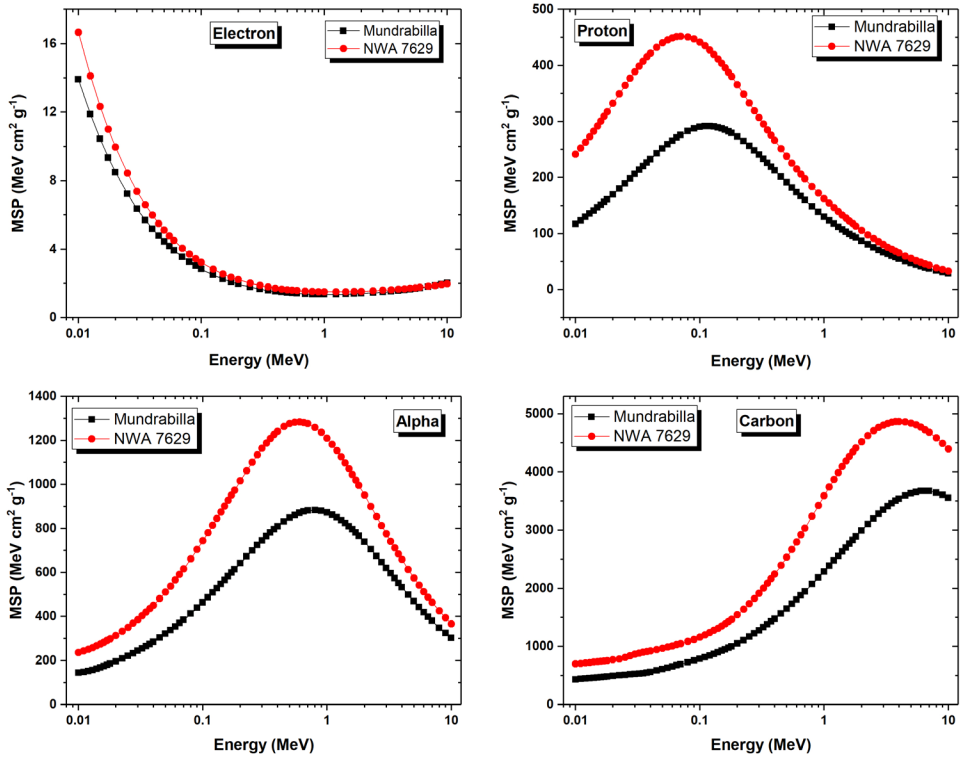


Figure 7: The MSP for charged particles as a function of energy for the Mundrabilla and NWA 7629 meteorites.

The projected/CSDA ranges for charged particles for Mundrabilla and NWA 7629 increase as energy enhances as presented in Figure 8. The projected/CSDA ranges for charged particles for NWA 7629 are higher than those of Mundrabilla.

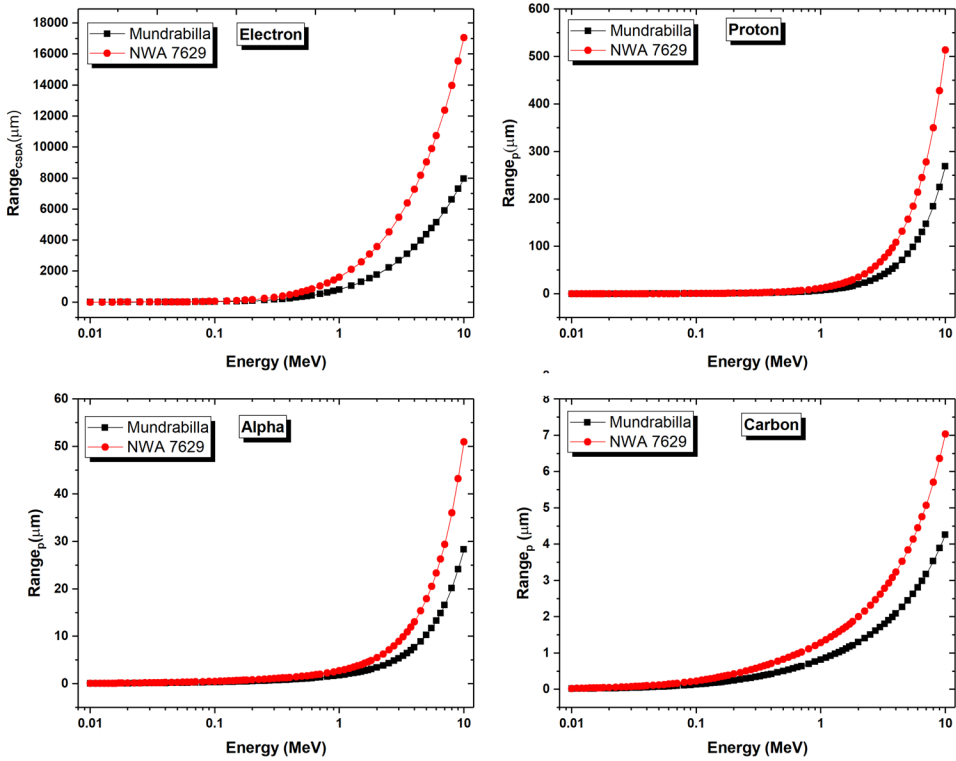


Figure 8: The projected/CSDA range for charged particles as a function of energy for the Mundrabilla and NWA 7629 meteorites.

Furthermore, the FNRCs are 0.15617 cm^{-1} for Mundrabilla and 0.10036 cm^{-1} for NWA 7629, thus the fast neutron attenuation of Mundrabilla is better than the fast neutron attenuation capability of NWA 7629.

4. CONCLUSION

The μ , μ/ρ , HVL, TVL, MFP, RPE, Z_{eff} , N_{eff} , Z_{eq} , C_{eff} , EBF and were obtained theoretically to determine photon attenuation properties of Mundrabilla and NWA 7629. Also, FNRCs were obtained for Mundrabilla and NWA 7629. In addition to these parameters, MSP and projected/CSDA range for charged particles were calculated theoretically for Mundrabilla and NWA 7629. The μ values of Mundrabilla are higher than the μ values of NWA 7629. The μ and μ/ρ values of Mundrabilla and NWA 7629 meteorites decrease with increasing photon energy. The HVLs, TVLs and MFPs of NWA 7629 are higher than those of Mundrabilla. The RPEs of the Mundrabilla are higher than for NWA 7629.

The Z_{eff} , N_{eff} , Z_{eq} and C_{eff} values of the Mundrabilla are nearly constant between 0.015 MeV and 15 MeV. The EBFs and EABFs decrease from 20 mfp to 1 mfp for both Mundrabilla and NWA 7629. The MSPs of NWA 7629 are higher than Mundrabilla for electrons up to 8 MeV however, at 9 and 10 MeV energies, the MSPs of Mundrabilla for electrons are higher than the MSPs of NWA 7629. The MSPs for proton, alpha and carbon of NWA 7629 are higher than those of Mundrabilla. The projected/CSDA ranges of charged particles for NWA 7629 are higher than those of Mundrabilla.

High energy particles with energies from 10 MeV/n to 10 GeV/n (energy per nucleon, not total energy) are significant for radiation exposure risk. These particles produce numerous secondary radiations including neutrons due to the nuclear fragmentation reactions with materials. Charged particle attenuation properties were studied between 10 keV to 10 MeV in this paper. In future studies, charged particle attenuation properties of the materials must be studied between 10 MeV/n to 10 GeV/n (energy per nucleon, not total energy).

Consequently, photon, fast neutron and charged particles attenuation capability of Mundrabilla are better than NWA 7629 due to the nickel content, higher density and higher content of iron. Obtained parameters vary depending on the density and elemental content of the Mundrabilla and NWA 7629.

5. REFERENCES

1. Bischoff, A. (2001). Meteorite classification and the definition of new chondrite classes as a result of successful meteorite search in hot and cold deserts. *Planet. Space Sci.*, 49, 769–776. [https://doi.org/10.1016/S0032-0633\(01\)00026-5](https://doi.org/10.1016/S0032-0633(01)00026-5)
2. Nabawy, B. S. & Rochette, P. A. (2016). A Preliminary study on the electrical signatures of some iron and stony meteorites and their dependence on nickel content. *Acta Geophys.*, 64(5), 1942–1969. <https://doi.org/10.1515/acgeo-2016-0055>
3. Arnold, J. R. (1961). Nuclear effects of cosmic rays in meteorites. *Annu. Rev. Nucl. Sci.*, 11,349–370. <https://doi.org/10.1146/annurev.ns.11.120161.002025>
4. Yavnel, A. A. (1960). Classification of meteorites according to their chemical composition. *Int. Geol. Rev.*, 2(5), 380–396. <https://doi.org/10.1080/00206816009473575>
5. Petrovic, J. J. (2001). Review mechanical properties of meteorites and their constituents. *J. Mater. Sci.*, 36,1579–1583. <https://doi.org/10.1023/A:1017546429094>
6. Elkins-Tanton, L. T. (2006). *Asteroids, meteorites and comets*. Newyork, United States of America: Chelsea House Publishers

7. Weisberg, M. K. et al. (2006). Systematics and evaluation of meteorite classification. In D. S. Lauretta & H. Y. Jr. Sween (Ed.). *Meteorites and the early solar system II*. Tucson: University of Arizona Press, 19–52.
8. Ozdin, D. et al. (2015). Mineralogy, petrography, geochemistry, and classification of the Kosice meteorite. *Meteorit Planet Sci.*, 50, 864–879. <https://doi.org/10.1111/maps.12405>
9. Dell’Aglia, M. et al. (2010). Laser induced breakdown spectroscopy applications to meteorites: Chemical analysis and composition profiles. *Geochim. Cosmochim. Acta.*, 74, 7329–7339. <https://doi.org/10.1016/j.gca.2010.09.018>
10. Clayton, R. N. et al. (1976). A classification of meteorites based on oxygen isotopes. *Earth Planet. Sci.*, 30(1), 10–18. [https://doi.org/10.1016/0012-821X\(76\)90003-0](https://doi.org/10.1016/0012-821X(76)90003-0)
11. Ray, D. et al. (2017). Petrography, classification, oxygen isotopes, noble gases, and cosmogenic records of Kamargaon (L6) meteorite: The latest fall in India. *Meteorit Planet Sci.*, 52(8), 1744–1753. <https://doi.org/10.1111/maps.12875>
12. Gemelli, M. et al. (2014). Chemical analysis of iron meteorites using a hand-held x-ray fluorescence spectrometer. *Geostand. Geoanalytical Res.*, 39(1), 55–69. <https://onlinelibrary.wiley.com/journal/1751908x>
13. Sears, D. W. G. et al. (2016). X-ray computed tomography imaging: A not-so-nondestructive technique. *Meteorit Planet Sci.*, 51(4), 833–838. <https://doi.org/10.1111/maps.12622>
14. Alexeev, V. A. et al. (2019). Cosmogenic radionuclides in meteorites and solar modulation of galactic cosmic rays in the internal heliosphere. *Sol. Syst. Res.*, 53(2), 98–115. <https://doi.org/10.1134/S0038094619010015>
15. Komura, K. et al. (2002). Cosmogenic radionuclides in the recently fallen Kobe (CK4) meteorite. *Geochem. J.*, 36(4), 333–340. <https://doi.org/10.2343/geochemj.36.333>
16. Kurudirek, M. et al. (2011). Analysis of some Earth, Moon and Mars samples in terms of gamma ray energy absorption buildup factors: Penetration depth, weight fraction of constituent elements and photon energy dependence. *Radiat. Phys. Chem.*, 80(3), 354–364. <https://doi.org/10.1016/j.radphyschem.2010.10.001>
17. Ferguson, H. & Gardner, W. H. (1962). Water content measurement in soil columns by gamma ray absorption. *Soil Sci. Soc. Am. J.*, 26(1), 11–14. <https://doi.org/10.2136/sssaj1962.03615995002600010004x>
18. Topp, G. C. (1970). Soil water content from gamma ray attenuation: A comparison of ionization chamber and scintillation detectors. *Can. J. Soil Sci.*, 50, 439–447.
19. Reinhardt, N. & Herrmann, L. (2019). Gamma-ray spectrometry as versatile tool in soil science: A critical review. *J. Plant. Nutr. Soil Sci.*, 182, 9–27. <https://doi.org/10.1002/jpln.201700447>
20. Costa, J. C. et al. (2014). Effect of collimator size and absorber thickness on soil bulk density evaluation by gamma-ray attenuation. *Radiat. Phys. Chem.*, 95, 333–335. <https://doi.org/10.1016/j.radphyschem.2012.11.013>

21. Pires, L. F. et al. (2020). Gamma ray attenuation for determining soil density: Laboratory experiments for environmental physics and engineering courses. *Rev. Bras. de Ensino de Fis.*, 42, e20190340. <https://doi.org/10.1590/1806-9126-RBEF-2019-0340>
22. Ellis, D. V. et al. (1987). Nuclear techniques for subsurface geology. *Annu. Rev. Nucl. Part. Sci.*, 37, 213–241. <https://doi.org/10.1146/annurev.ns.37.120187.001241>
23. Pires, L. F. & Pereira, A. B. (2014). Gamma-ray attenuation to evaluate soil porosity: An analysis of methods. *Sci. World J.*, 723041. <https://doi.org/10.1155/2014/723041>
24. Oliveira, J. C. M. et al. (1998). Soil structure evaluated by gamma-ray attenuation. *Soil Tillage Res.*, 48, 127–133. [https://doi.org/10.1016/S0167-1987\(98\)00130-5](https://doi.org/10.1016/S0167-1987(98)00130-5)
25. Peplowski, P. N. et al. (2018). Characterizing near-surface elemental layering on Mars using gamma-ray spectroscopy: A proof-of-principle experiment. *Nucl. Instrum. Methods Phys. Res. B*, 415, 89–99. <https://doi.org/10.1016/j.nimb.2017.11.016>
26. Evans, L. G. et al. (2015). Chlorine on the surface of Mercury: MESSENGER gamma-ray measurements and implications for the planet's formation and evolution. *Icarus*, 257, 417–427. <https://doi.org/10.1016/j.icarus.2015.04.039>
27. Peplowski, P. N. et al. (2015). Geochemical terranes of Mercury's northern hemisphere as revealed by MESSENGER neutron measurements. *Icarus*, 253, 346–363. <https://doi.org/10.1016/j.icarus.2015.02.002>
28. Lawrence, D. J. et al. (2017). Compositional terranes on Mercury: Information from fast neutrons. *Icarus*, 281, 32–45. <https://doi.org/10.1016/j.icarus.2016.07.018>
29. Beck, A. W. et al. (2015). Using HED meteorites to interpret neutron and gamma-ray data from asteroid 4 Vesta. *Meteorit. Planet. Sci.*, 50 (8), 1311–1337. <https://doi.org/10.1111/maps.12467>
30. Abdullah, K. K. et al. (2010). X-ray attenuation around K-edge of Zr, Nb, Mo and Pd: A comparative study using proton-induced x-ray emission and ^{241}Am gamma rays. *Pramana*, 75(3), 459–469. <https://doi.org/10.1007/s12043-010-0131-7>
31. Christmas, P. (1974). Measurement of γ -ray attenuation coefficients. *Int. J. Appl. Radiat. Isot.*, 25(1), 25–29. [https://doi.org/10.1016/0020-708X\(74\)90050-7](https://doi.org/10.1016/0020-708X(74)90050-7)
32. Hubbell, J. H. (1982). Photon mass attenuation and energy-absorption coefficients. *Int. J. Appl. Radiat. Isot.*, 33(11), 1269–1290. [https://doi.org/10.1016/0020-708X\(82\)90248-4](https://doi.org/10.1016/0020-708X(82)90248-4)
33. Mohammed, F. M. et al. (2013). X-ray mass attenuation coefficients for mixture of some 3d elements $\text{Fe}_{100-x}\text{-Al}_x$ and $\text{Cu}_{100-x}\text{-Al}_x$. *Aust. J. Basic. Appl. Sci.*, 7(4), 810–815.
34. Haghghi, R. R. et al. (2011). X-ray attenuation coefficient of mixtures: Inputs for dual-energy CT. *Med. Phys.*, 38(10), 5270–5279. <https://doi.org/10.1118/1.3626572>

35. Singh, K. et al. (1996). Study of effective atomic numbers and mass attenuation coefficients in some compounds. *Radiat. Phys. Chem.*, 47(4), 535–541. [https://doi.org/10.1016/0969-806X\(95\)00057-5](https://doi.org/10.1016/0969-806X(95)00057-5)
36. Parthasaradhi, K. et al. (1992). Photon attenuation coefficients in tissue equivalent compounds. *Int. J. Radiat. Appl. Instrum. Part A, Appl. Radiat. Isot.*, 43(12), 1481–1484. [https://doi.org/10.1016/0883-2889\(92\)90175-E](https://doi.org/10.1016/0883-2889(92)90175-E)
37. Manjunath, A. et al. (2020). Determination of Mass Attenuation Coefficient for some Technetium-99m Compounds. *Macromol. Symp.*, 393, 2000095. <https://doi.org/10.1002/masy.202000095>
38. Sayyed, M. I. et al. (2019). Evaluation of radiation absorption capacity of some soil samples. *Radiochim. Acta*, 107(1), 83–93. <https://doi.org/10.1515/ract-2018-2996>
39. Hila, F. C. et al. (2021). Evaluation of photon radiation attenuation and buildup factors for energy absorption and exposure in some soils using EPICS2017 library. *Nucl. Eng. Technol.*, 53(11), 3808–3815. <https://doi.org/10.1016/j.net.2021.05.030>
40. Eke, C. (2021). Investigation of gamma-ray attenuation properties of beach sand samples from Antalya, Turkey. *Arab. J. Geosci.*, 14(3), 159. <https://doi.org/10.1007/s12517-020-06413-4>
41. Akman, F. et al. (2019). Evaluation of radiation absorption characteristics in different parts of some medicinal aromatic plants in the low energy region. *Results Phys.*, 12, 94–100. <https://doi.org/10.1016/j.rinp.2018.11.055>
42. Eke, C. et al. (2017). Attenuation properties of radiation shielding materials such as granite and marble against gamma-ray energies between 80 and 1350 keV. *Radiochim. Acta*, 105(10), 851–863. <https://doi.org/10.1515/ract-2016-2690>
43. Al-Hamarneh, I. F. (2017). Investigation of gamma-ray shielding effectiveness of natural marble used for external wall cladding of buildings in Riyadh, Saudi Arabia. *Results Phys.*, 7, 1792–1798. <https://doi.org/10.1016/j.rinp.2017.05.017>
44. Elsafi, M. et al. (2021). Shielding properties of some marble types: A comprehensive study of experimental and XCOM results. *Mater.*, 14, 4194. <https://doi.org/10.3390/ma14154194>
45. Mahmoud, K. A. et al. (2019). Gamma ray shielding characteristics and exposure buildup factor for some natural rocks using MCNP-5 code. *Nucl. Eng. Technol.*, 51(7), 1835–1841. <https://doi.org/10.1016/j.net.2019.05.013>
46. Olukotun, S. F. et al. (2018). Investigation of gamma radiation shielding capability of two clay materials. *Nucl. Eng. Technol.*, 50(6), 957–962. <https://doi.org/10.1016/j.net.2018.05.003>
47. Bashter, I. I. (1997). Calculation of radiation attenuation coefficients for shielding concretes. *Ann. Nucl. Energy*, 24(17), 1389–1401. [https://doi.org/10.1016/S0306-4549\(97\)00003-0](https://doi.org/10.1016/S0306-4549(97)00003-0)
48. Ouda, A. S. & Abdelgader, H. S. (2019). Assessing the physical, mechanical properties, and γ -ray attenuation of heavy density concrete for radiation shielding purposes. *Geosystem Eng.*, 22(2), 72–80. <https://doi.org/10.1080/12269328.2018.1469434>

49. Al-Buriahi, M. S. et al. (2021). Radiation attenuation properties of some commercial polymers for advanced shielding applications at low energies. *Polym Adv Technol.*, 32(6), 2386–2396. <https://doi.org/10.1002/pat.5267>
50. Nagaraja, N. et al. (2020). Radiation shielding properties of silicon polymers. *Radiat. Phys. Chem.*, 171, 108723. <https://doi.org/10.1016/j.radphyschem.2020.108723>
51. Alothman, M. et al. (2021). The significant role of CeO₂ content on the radiation shielding performance of Fe₂O₃-P₂O₅ glass-ceramics: Geant4 simulations study. *Phys. Scr.*, 96(11), 115305–115305. <https://doi.org/10.1088/1402-4896/ac1028>
52. Almatari, M. (2019). Gamma radiation shielding properties of glasses within the TeO₂-TiO₂-ZnO system. *Radiochim. Acta.*, 107(6), 517–522. <https://doi.org/10.1515/ract-2018-3058>
53. Japari, S. J. et al. (2021). Effects of Na₂O on optical and radiation shielding properties of xNa₂O-(20-x)K₂O-30V₂O₅-50TeO₂ mixed alkali glasses. *Results Phys.*, 22, 103946. <https://doi.org/10.1016/j.rinp.2021.103946>
54. Kim, M. H. Y. et al. (1998). Comparison of Martian Meteorites and Martian Regolith as shield materials for galactic cosmic rays. National Aeronautics and Space Administration, NASA/TP-1998-208724, Langley Research Center, Hampton, Virginia.
55. Moreira, A. C. & Appoloni, C. R. (2006). Mass attenuation coefficient of the Earth, Moon and Mars samples over 1keV–100GeV energy range. *Appl. Radiat. Isot.*, 64(9), 1065–1073. <https://doi.org/10.1016/j.apradiso.2006.04.002>
56. Honda, M. & Arnold, J. R. (1964). Effects of cosmic rays on meteorites. *Sci.*, 143(3603), 203–212. <https://doi.org/10.1126/science.143.3603.203>
57. Adams, J. H. et al. (2005). Revolutionary concepts of radiation shielding for human exploration of space. National Aeronautics and Space Administration, Marshall Space Flight Center, NASA/TM-2005-213688, Alabama.
58. Wilson, J. W. et al. (1999). Shielding from solar particle event exposures in deep space. *Radiat. Meas.*, 30(3), 361–382. [https://doi.org/10.1016/S1350-4487\(99\)00063-3](https://doi.org/10.1016/S1350-4487(99)00063-3)
59. Kennedy, A. R. (2014). Biological effects of space radiation and development of effective counter measures. *Life Sci. Space Res.*, 1, 10–43. <https://doi.org/10.1016/j.lssr.2014.02.004>
60. Naito, M. et al. (2020). Investigation of shielding material properties for effective space radiation protection. *Life Sci. Space Res.*, 26, 69–76. <https://doi.org/10.1016/j.lssr.2020.05.001>
61. Zhang, Y. et al. (2021). Ti₃C₂Tx/rGO porous composite films with superior electromagnetic interference shielding performances. *Carbon*, 175, 271–280. <https://doi.org/10.1016/j.carbon.2020.12.084>
62. Chinnappa Redd, B. et al. (2021). X-ray/gamma ray radiation shielding properties of α-Bi₂O₃ synthesized by low temperature solution combustion method. *Nucl. Eng. Technol.*, in press. <https://doi.org/10.1016/j.net.2021.09.023>

63. Sakar, E. et al. (2020). Phy-X/PSD: Development of a user friendly online software for calculation of parameters relevant to radiation shielding and dosimetry. *Radiat. Phys. Chem.*, 166, 108496. <https://doi.org/10.1016/j.radphyschem.2019.108496>
64. Berger, M. et al. (1999). ESTAR, PSTAR, and ASTAR: Computer programs for calculating stopping-power and range tables for electrons, protons, and helium ions (version 1.21). <http://physics.nist.gov/Star>, [online] (Accessed 05 August 2021).
65. Ziegler, J. F. (2004). SRIM-2003. *Nucl. Instrum. Methods Phys. Res. B: Beam Interact. Mater. At.*, 219–220, 1027–1036. <https://doi.org/10.1016/j.nimb.2004.01.208>
66. Ziegler, J. F. et al. (2010). SRIM—the stopping and range of ions in matter. *Nucl. Instrum. Methods Phys. Res. B: Beam Interact. Mater. At.*, 268(11–12), 1818–1823. <https://doi.org/10.1016/j.nimb.2010.02.091>
67. Gili, M. B. Z. & Hila, F. C. (2021). Characterization and radiation shielding properties of Philippine natural bentonite and zeolite. *Philipp J. Sci.*, 150(6A), 1475–1488.
68. Grimes, D. R. et al. (2017). An approximate analytical solution of the Bethe equation for charged particles in the radiotherapeutic energy range. *Sci. Rep.*, 7, 9781. <https://doi.org/10.1038/s41598-017-10554-0>
69. Kurudirek, M. (2021). Heavy metal borate glasses: Potential use for radiation shielding. *J. Alloys Compd.*, 727, 1227–1236. <https://doi.org/10.1016/j.jallcom.2017.08.237>